The next generation radio telescopes/ Les radiotélescopes du futur

Blind Detection of Giant Pulses: GPU Implementation

Dalal Ait-Allal [a], Rodolphe Weber [b,a], Cédric Dumez-Viou [a], Ismael Cognard [c],
Gilles Theureau [a,c]

[a] Observatoire de Paris, Station de radioastronomie de Nançay, F-18330 Nançay, France
[b] Laboratoire PRISME, Université d'Orléans, Site Galilée, 12 rue de Blois, 45067 Orléans cedex 2, France
[c] Laboratoire de Physique et Chimie de l'Environnement et de l'Espace, Université d'Orléans / CNRS, 3, Avenue de la
Recherche Scientifique, 45045 Orléans cedex, France

Abstract

Radio astronomical pulsar observations require specific instrumentation and dedicated signal processing to cope with the dispersion caused by the interstellar medium. Moreover, the quality of observations can be limited by radio frequency interferences (RFI) generated by Telecommunications activity. This paper will present the innovative pulsar instrumentation based on Graphical Processing Units (GPU) which has been designed at the Nançay Radio Astronomyl Observatory. In addition, for giant pulsar search, we propose a new approach which combines a hardware-efficient search method and some RFI mitigation capabilities. Although this approach is less sensitive than the classical approach, its advantage is that no a priori information on the pulsar parameters is required. The validation of a GPU implementation is under way. *To cite this article: D. Ait-Allal, R. Weber, C. Dumez-Viou, I.Cognard, G.Theureau, C. R. Physique 13 (2012).*

Résumé

Détection Aveugle de Pulses Géants : Implantation sur GPU. L'observation radio des pulsars nécessite une instrumentation spécifique et des procédures de traitement du signal dédiées qui corrigent les effets de la dispersion induite par le milieu interstellaire. En outre, la qualité des observations peut être notablement dégradée par la présence d'interférences radioélectriques (RFI) d'origine anthropique. Ce papier présente l'instrumentation mise en place pour l'observation des pulsars à la Station de Radioastronomie de Nançay. Notamment, nous détaillons une approche originale pour la détection automatique de pulses géants. Bien que moins sensible que l'approche classique consistant à balayer en temps différé l'espace des paramètres du pulsar potentiel, l'approche proposée se distingue par une efficacité d'implantation, une capacité de traitement en temps réel et une robustesse intrinsèque aux RFI. En outre, elle ne nécessite aucune connaissance préalable des paramètres du pulsar, ce qui autorise son utilisation pour la détection d'événements impulsionnels non répertoriés. Une implantation sur GPU est en cours de validation. *Pour citer cet article : D. Ait-Allal, R. Weber, C. Dumez-Viou, I.Cognard, G.Theureau, C. R. Physique 13 (2012).*

Key words: RFI mitigation ; Pulsar ; transient detection ; GPU

Mots-clés : Elimination des RFI ; Pulsar ; détection de signaux impulsionnels ; GPU

1. Introduction

Pulsars are rapidly rotating (up to 716 rotations per second) highly magnetized, neutron stars which produce radio beams which sweep the sky like a lighthouse. If the beam is oriented towards the Earth, it will produce periodic pulses which can be measured with radio telescopes and dedicated backends [1]. As they travel through the ionized interstellar medium (ISM), these pulses are progressively attenuated and spread over time (i.e. the higher pulsar frequencies will arrive earlier than the lower pulsarfrequencies). Figure 1.a shows a raw time-frequency representation of one of these pulses. This phenomenon, named dispersion, makes these pulses barely detectable without further processing. Moreover, the quality of pulsar observations is also limited by radio frequency interferences (RFI) generated by various (and growing) Telecommunications activities. Figure 1.c gives an example of the distortion induced by RFI on pulsar observation (to be compared with Figure 1.b). To cope with RFI, different RFI blanking techniques can be implemented. Examples of RFI mitigation procedures are given in [2,3].

In section 2, the functional description of the coherent dedispersion algorithm is explained and the innovative hardware architecture of the Nançay de-dispersion backend is detailed. When both the dispersion measure (DM,i.e. the integrated column density of free electrons between an observer and a pulsar) and the period of the pulsar are known, this architecture makes a precise timing of the corresponding pulsar possible.

The search for new pulsars is a difficult task since neither the DM nor the periodicity are known. The classical approach consists in recording all the channelized data and in incoherently de-dispersing them by an off-line search in the DM space. Finally, all the data are folded with different sets of periods, providing a list of pulsar candidates. This approach requires huge disk space and is quite time consuming.

In section 3, we propose a new real time pulsar search method, requiring small disk space, fewer computational resources and providing a simple way to blank RFI. Its advantage is that no a priori information on the pulsar parameters is required.

As will be shown in sections 4 and 5, the drawback is that this approach is less sensitive than the classical approach mentioned above. Consequently, the proposed approach is well adapted to high dynamic transient emissions such as Rotating radio transients (RRATs, short and bright single pulses observed one at a time with the average time intervals between bursts ranging from a few minutes to several hours[4]) or giant pulses (very bright pulses occurring from time to time [5,6]).

In section 6, the GPU implementation of this algorithm is described.

2. The coherent de-dispersion receiver

2.1. *Coherent de-dispersion principle*

ISM dispersion can be modeled as a frequency transfer function [1], $H(f)$:

$$H(f + f_0) = exp(j\frac{2\pi DM f^2}{2.41 \times 10^{-10}(f + f_0)f_0^2})$$ (1)

where f_0 is the center frequency of observed bandwidth Δf and $|f| < \Delta f/2$. Coherent de-dispersion consists in applying the inverse of this transfer function to the dispersed received signal. This de-dispersion

----

Email addresses: `dalal.ait_allal@obs-nancay.fr` (Dalal Ait-Allal), `rodolphe.weber@univ-orleans.fr` (Rodolphe Weber), `cedric.dumez-viou@obs-nancay.fr` (Cédric Dumez-Viou), `icognard@cnrs-orleans.fr` (Ismael Cognard), `theureau@obs-nancay.fr` (Gilles Theureau).
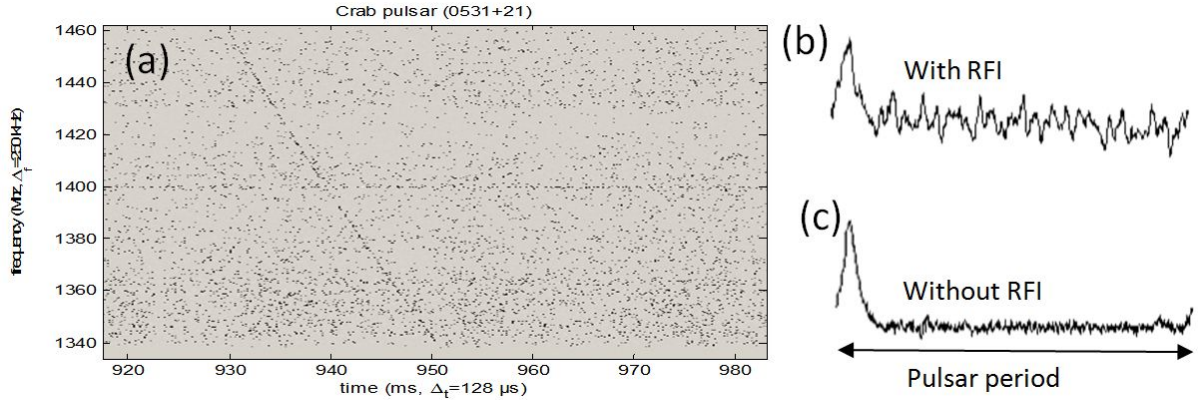
Figure 1. Pulsar examples. (a) Time-frequency representation of one giant pulse of the Crab pulsar (b) Time representation of the average power pulse profile (pulsar J0034-0721) after coherent de-dispersion but with RFI signals present in the observed band. (c) Time representation of the average power pulse profile of the pulsar J0034-0721 after coherent de-dispersion and with RFIs blanked out.

is done in the complex frequency domain through Fourier transforms. The operations are detailed inside the Data server box in Figure 2.a. A taper function is used to avoid aliasing in the low-pass filtering.

2.2. *Receiver hardware implementation*

Figure 2 shows the signal data-flow from the radio telescope to the final de-dispersed pulses. The different steps are described below:

- The Analog System: two orthogonal polarization signals (500 MHz bandwidth) from the radio telescope are downconverted for analog to digital conversion and channelizing.
- The ROACH Board (cf. Figure 2.b and [7]): This digital board was designed by CASPER (Center For Astronomy Signal Processing and Electronics Research). For this application, it contains two 8-bit analog to digital converters (ADCs) which are clocked at 1024MSa/s. A logic programmable device (Virtex 5 SX95T from Xilinx) is used to perform a 128 channel polyphase filter bank (PFB). Each channel output bandwidth of complex data samples is 4 MHz.
- Data servers (cf. Figure 2.c): This is the innovative part of the design. 4 PCs embedding 2 GPUs each (Graphic Processing Unit- NVIDIA GT280 240 parallel processors) are used for the final processing steps. Each PC receives a quarter of the bandwidth through 10 GbE (Gigabit Ethernet) links. The data are then read by the de-dispersion program which performs the following tasks:
    - Convert raw data from proprietary fixed point format to floating point.
    - Apply a Fourier transform of appropriate length (256k bins).
    - Multiply by the de-dispersion filter, $H(f)^{-1}$ and the taper function
    - Inverse Fourier transform back to the time domain.
    - Detect the data to obtain power versus time, and crossmultiply polarization terms.
    - Folding at the pulsar period with a 60 s dump time.
- Channel integration to enhance the sensitivity.

This system is now fully operational at Nançay Observatory. In terms of sensitivity, it outperforms the previous system presented in [2] by a factor of 2.
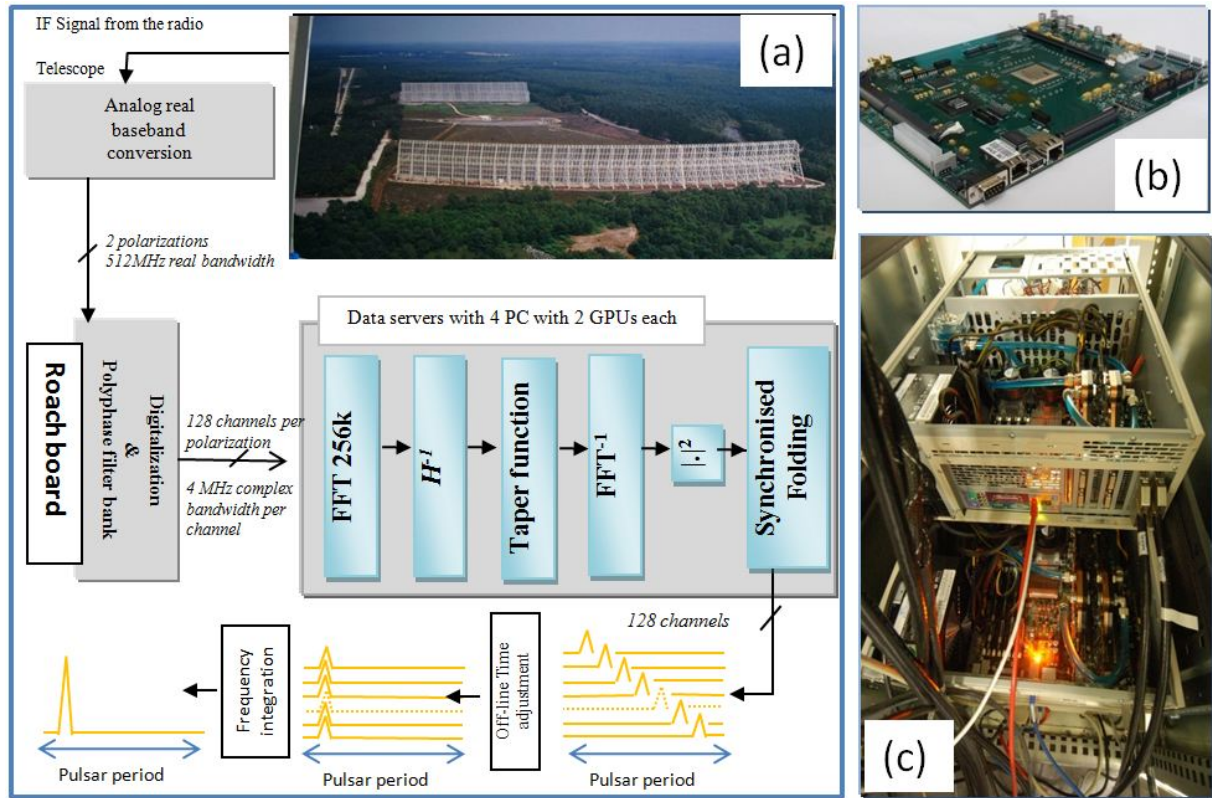
3

Figure 2. Nançay coherent pulsar receiver. (a) Description of the instrumentation. (b) ROACH digital board for the waveform digitization and the polyphase filter bank. (c) 'data servers' with 4×2 GPUs which compute the coherent de-dispersion and the synchronized folding on each frequency channel.

3. The giant pulse blind detector

In Figure 3, the different steps of the algorithm are presented and an example with a real pulsar pulse is provided for illustration. In short :
– After analog to digital conversion, a time-frequency (t-f) power plane of the waveform is produced through a digital filter bank (see an example on Figure 3.b). This is a regular real-time functionality in all radio telescopes.
– To remove obvious RFI, t-f slots with high levels are truncated. A simple power detector with a coarse threshold can be implemented. If computational resources are available, a more sophisticated approach may be chosen [8,9].
– Real time 2D Fourier transforms (2D-FFT) are applied on successive $N \times N$ t-f images. An example is given in Figure 3.c. With this approach, all the dispersed pulsar pulses are projected at the same location in the 2D-FFT image. This location depends only on the pulsar DM and is different from the one obtained for RFI. In other words, any impulsive (respectively continuous) RFI will be concentrated in the horizontal (resp. vertical) line centered in the 2D-FFT image. Thus, to remove RFI and to obtain a clean image, all that is required is to blank these vertical and horizontal lines which cross at the center of the 2D-FFT image.
– A Radon transform is applied on the cleaned 2D-FFT image. It consists in summing the image
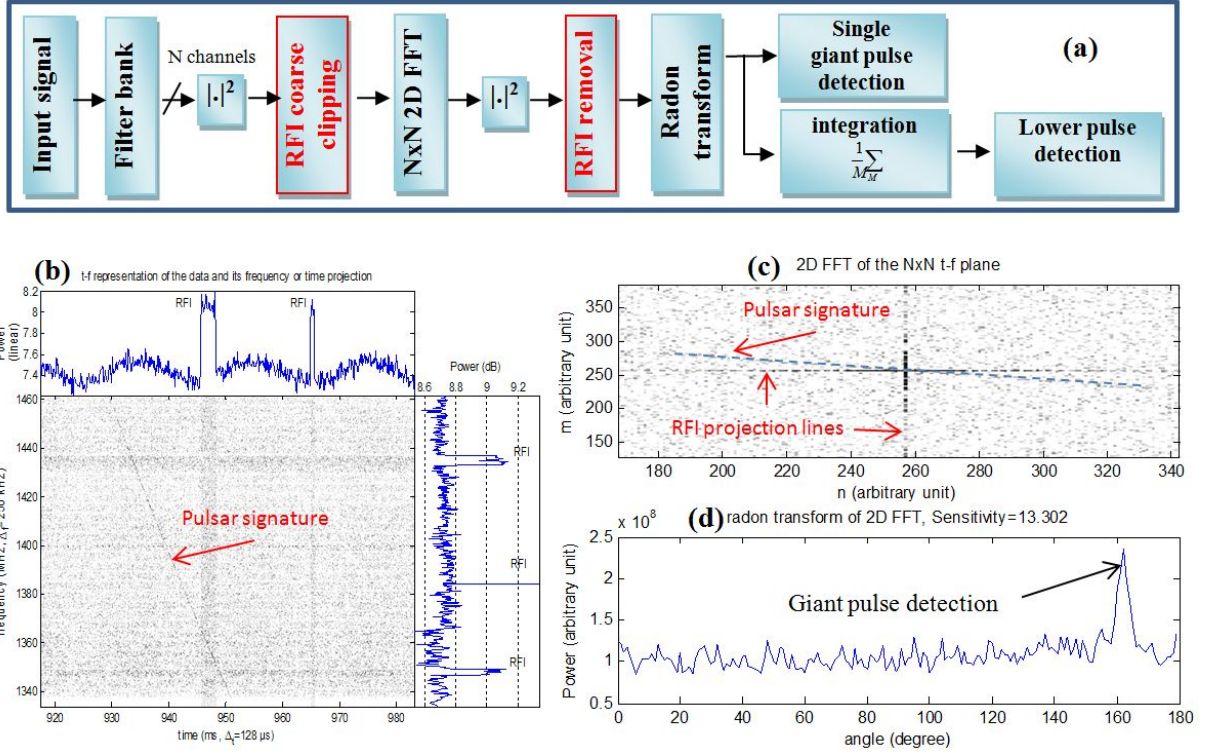
4

Figure 3. (a) Algorithm description. (b) Time-frequency (t-f) representation ($N = 512$) of the signal. On the integrated power figures (top and right), the time and frequency RFI positions can be easily located. The 3 RFI spectral lines and the 2 RFI time bursts are simulated RFIs. The dispersed pulse is emitted by the Crab pulsar. (c) Example of the 2D-FTT ouput (zoomed in). All the RFI are concentrated on the central cross. The oblique line is the signature of a dispersed pulse. Its angle depends on the pulsar DM. (d) Radon transform of the previous cleaned 2D-FTT plane (i.e. the central cross has been blanked). The peak indicates the presence of a pulse. The result is strictly similar if there is no RFI.

intensity along successive radial lines [10]. When this integration line corresponds to the line where the pulsar pulses have been projected, all the pulsar power is concentrated in one point. At other integration angles, only the noise contribution will be integrated. Figure 3.d illustrates this principle.

The advantage of this approach is that only a limited amount of data (the Radon profile of the $N \times N$ 2D-FFT image) is stored for further processing. Furthermore, it provides simple RFI mitigation capabilities. The successive Radon profiles can also be integrated over time to enhance the detection of pulses. In the following, we investigate the sensitivity of this 2D-FTT/Radon approach compared with the classical one (i.e. incoherent de-dispersion).

4. Sensitivity comparison

We consider the following signal model and algorithm parameters:
– The background noise is a white zero-mean Gaussian noise with power σ_n^2.
– The pulsar pulse is a white zero-mean Gaussian noise with power σ_p^2. The pulse duration is L. The signal to noise ratio is defined by $SNR = \sigma_p^2/\sigma_n^2$. For the theoretical sensitivity derivation, we assume that $\sigma_p^2 \ll \sigma_n^2$.
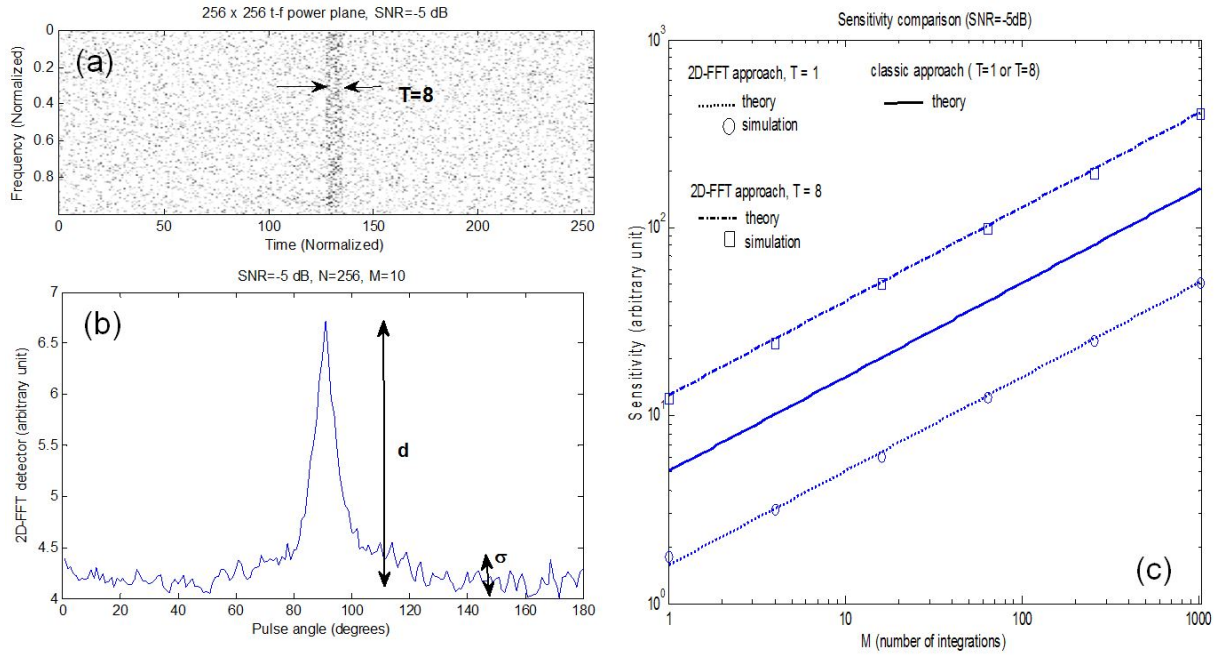
5

Figure 4. Comparison of the 2D-FFT and the classical pulsar search procedures ($N = 256$, $SNR = -5$ dB). Two pulse lengths ($T = 1$ and $T = 8$ in samples) were simulated for different values of M. (a) Model of the t-f plane used for the simulations. (b) Graphical definition of the parameters used to compute the sensitivity. (c) Sensitivities for different values of T and M. The continuous and dashed curves correspond to theoretical values. Boxes and circles correspond to 2D-FFT sensitivity measurements through simulations.

– There is no RFI.
– The t-f power plane size is $N \times N$. The time and frequency units are normalized.
– For the classical approach, we consider that the DM and the pulsar periodicity have been found by the ad-hoc iterative procedure. Thus, it is equivalent to assuming 1) DM=0 (*i.e.* vertical pulse) and 2) pulses always occur at the same position in the t-f power plane. These t-f power planes are integrated over frequency to provide individual pulse profiles. Finally, M pulse profiles are summed together. The sensitivity, $S_{classic}$, is defined by the average profile deviation due to the pulse over the noise only profile standard deviation.
– For the 2D-FFT approach, we set DM to zero as well. Indeed, with no loss of generality, we consider that zero-DM is just a DM among others. The central pixel of the 2D-FFT image is systematically blanked. The average of M 2D-FFT planes provides the final clean 2D-FFT image. Finally, the Radon transform is applied for different angles. The sensitivity, S_{2DFFT} is defined by the Radon transform deviation at angle 90 over the Radon transform standard deviation at other angles.

This model is illustrated in Figure 4.a. A graphical definition of sensitivity is provided in Figure 4.b. By considering the mean and the variance of this model at the successive algorithm stages, we have derived the following theoretical equations:

– for the classical case: $S_{classic} = \frac{\sigma_p^2}{\sigma_n^2/\sqrt{NM}} = SNR\sqrt{NM}$

– for the 2D-FFT case: $S_{2DFFT} = \frac{T\sigma_p^4}{\sigma_n^4/\sqrt{NM}} = T.SNR^2\sqrt{NM}$ where $T = L/N$ (*i.e.* T is the pulse width in the t-f power plane).

6

In Figure 4.c, these sensitivities were computed by simulation for different parameters. Theoretical sensitivities are also plotted. From this figure, several remarks can be made:

– It is shown that there is good agreement between theory and simulations.
– The 2D-FFT sensitivity is proportional to SNR^2. This makes this approach less sensitive to low SNR compared with the classical approach (see for example the case ($SNR = -5$ dB, $T = 1$)). This drawback is counterbalanced by the fact that the 2D-FFT approach is also sensitive to the pulse width, T. The wider the pulse is, the better the 2D-FFT detection is (see case ($SNR = -5$ dB, $T = 8$)).
– These detection performances are achieved without requiring any prior knowledge about the pulsar (neither the DM nor the periodicity). This is not the case for the classical pulsar search procedure, where the derived performances are only achieved when exact DM and periodicity are known.

5. Tests on Crab pulsar data

The two detectors were applied to a Crab pulsar data set acquired with the Nançay Decimeter Radio Telescope. This data set corresponds to 4452 t-f planes generated with the size parameter $N = 512$. The $N = 512$ frequency channels cover the band from 1.3339 GHz to 1.4619 GHz. The temporal resolution is 128 μs. Consequently, the total duration of the data set is 4 mn 55 s. The pulsar parameters applied for the incoherent de-dispersion process (classical approach) are $DM = 56.65 pc.cm^{-3}$ and period=33.63128 μs.

The classical approach is used to identify t-f planes with at least one pulse inside. The detection criteria are 'sensitivity above 4' and 'peak position at the expected pulse positions within the pulsar period'. In Figure 5.a, the black circles represent the 589 t-f planes fulfilling the previous detection thresholds. This set of t-f planes is called the H1 data set. The 3863 other t-f planes without pulse inside (small gray circles) are called the H0 data set. Figure 5.a on the right shows the averaged dedispersed pulse profile obtained from the H1 data set.

In Figure 5.b, the sensitivities measured in the H1 data set between the classical and the 2D-FFT approaches are compared. It can be seen that the 2D-FFT performance is appreciably lower than the expected theoretical one (see section 4). One reason is that real data sets are affected by propagation issues such as scintillation. Another one is that real pulse profiles are not perfectly rectangular as was assumed in section 4. However, the positive point is that with a sensitivity threshold around 6, the 2D-FFT detector is able to detect strong pulses with no false alarm. More precisely, 65 t-f planes provide 2D-FFT sensitivities above 6 (compared to the 365 classical detections obtained with the same sensitivity threshold). A first conclusion is that very strong Pulsar pulses can be detected with no false alarm and without any prior knowledge of the pulsar DM. Furthermore, the angle corresponding to the detection peak in the Radon profile provides a first estimate of the unknown pulsar DM.

Figures 5.c and 5.d show that detection with lower sensitivities can be achieved by integrating Radon profiles. Thus, Figure 5.c shows that by summing all the individual H1 Radon profiles with a sensitivity lower than a given sensitivity threshold, a new Radon profile can be generated with a better signal to noise ratio. For example, by integrating the 136 lowest individual H1 Radon profiles (i.e. sensitivity threshold =2.7), a zero false alarm detection is obtained (i.e. new sensitivity = 6). For this example, one individual profile (dashed red line) and the cumulative one (continuous blue line) are compared on Figure 5.d. Thus, the second conclusion is that the proposed approach can achieve positive detections of lower pulses by integrating the individual Radon profiles. Similarly, the classical detector can be enhanced by folding the dedispersed profile. However, the knowledge of pulsar period is required in that case.

This study on real data confirms that the 2D-FFT approach is an interesting alternative for the blind detection of strong pulses in real time.
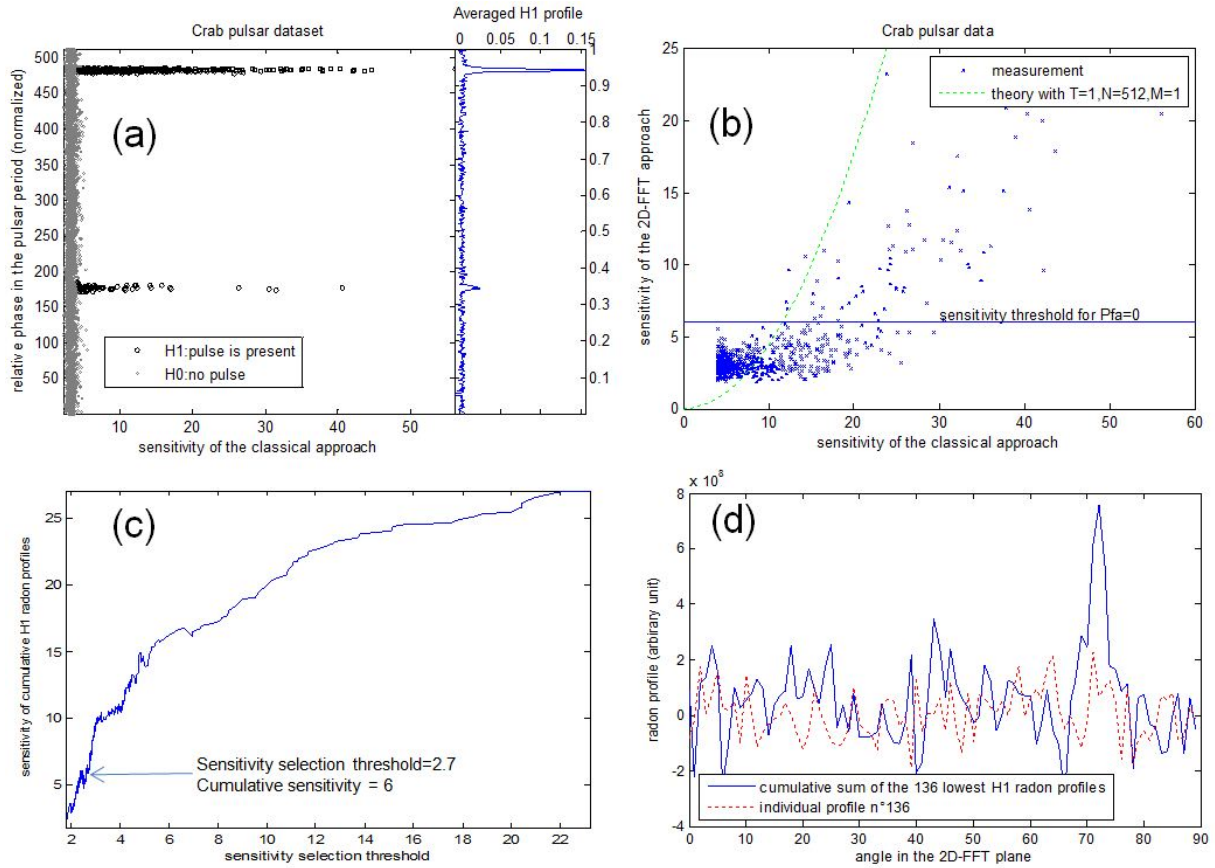
7

Figure 5. (a) Distribution of the 4452 t-f planes from the Crab pulsar data set. Classical (incoherent de-dispersion) sensitivities obtained versus the corresponding maximum position in the dedispersed pulse profile. Black circles indicate positive detections. The corresponding t-f planes are labelled H1 data set. Small gray circles represent the H0 data set with no pulse inside the t-f planes. The plot on the right gives the integrated pulse profile obtained with the H1 data set. (b) Sensitivity comparaison between the classical approach and the 2D-FFT approach with the H1 data set. The dashed line represents the theoretical relation between these sensitivities (see section 4). The horizontal line represents the positive detection limit providing a probability of false alarm (Pfa) equal to zero. (c) Sensitivity obtained after integration of all the individual Radon profiles with a sensitivity below a given threshold. (d) Comparison of individual and cumulative Radon profiles for the parameters indicated with an arrow on Figure 5.c.

6. GPU implementation

Performance tests were conducted to prove the effectiveness of GPUs as an appropriate solution to data processing for wider band and in real time [11]. The new blind detection method, it was implemented on a machine equipped with a GeForce GTX 85, with 240 cores, 1 GB of global memory and 16 MB of shared memory. The operating system is Gentoo Linux with CUDA library 2.3. The CUDA library is very well suited to exploiting the parallel computing capabilities of the GPU. Indeed, when the GPU is programmed through CUDA C, which is an extension of the C language, it becomes a computing device capable of performing a large number of parallel operations; an algorithm can be executed several times on several independent data sets. In the new method explained in Section 3, two steps are required for its implementation: the two-dimensional Fourier transform (FFT^2) and the Radon transform. The

8

FFT can be done with the CUFFT library which comes with CUDA C. In this section, we will therfore focus on the implementation of the Radon transform. In fact, the Radon transform is simply the sum of intensities in the image as a function of the radial lines through the center of the image. Call θ the angle of the radial with the horizontal. Due to the symmetry present in the output image of FFT^2, and in order to minimize the computation time, the Radon transform is applied on only a quarter of the image between $\theta = 0°$ and $\theta = 90°$. Then, for each value of θ, the pixels index of the corresponding radial line is calculated in advance. The K indexes of the N angles θ are then stored in an index matrix $(N \times K)$ and transferred once and for all in the shared memory of the GPU. This technique optimizes data transfer and improves processing speed. Finally, the sum of the intensities according to each row of the index matrix is calculated by the reduction algorithm, which is the sum of two by two elements at each stage,thus halving the number of calculations every time. The result is a vector containing the cumulative intensities for each value θ as shown in Figure 3.d.

7. Conclusions

A new approach for pulsar search, combining a hardware-efficient search method and some RFI mitigation capabilities has been proposed. It is based on two-dimensional Fourier transform and Radon transform. While this algorithm is less sensitive than the classical one based on incoherent de-dispersion, positive detection can be achieved on strong pulses without knowing the DM of the corresponding pulsar. It could be an alternative for the next generation of radio telescopes such as the LOFAR radio telescope (www.lofar.org) or the Square Kilometre Array (SKA, www.skatelescope.org) where the huge amount of data to be processed by classical search procedures is a serious issue.

References

[1] D. Lorimer and M. Kramer "Handbook of pulsar astronomy," Cambridge (GB): Cambridge University Press, 2005. pp. 106-123 and pp. 141-142.

[2] D. Ait-Allal, C. Dumez-Viou, R. Weber, G. Desvignes, I. Cognard, and G. Theureau,RFI mitigation at Nançay Observatory: Impulsive Signal Processing, Widefield Science and Technology for the SKA, S. A. Torchinsky, A. van Ardenne, T. van den Brink-Havinga, A. van Es, A.J. Faulkner (eds.), ISBN 978-90-805434-5-4, 2010.

[3] R. P. Eatough, E. F. Keane, and A. G. Lyne, An Interference Removal Technique for Radio Pulsar Searches, 2009, Mon. Not. R. Astron. Soc., 395,410.

[4] McLaughlin, M. A. et al. ,Transient radio bursts from rotating neutron stars, (2006)Nature 439 (7078): 817820

[5] D.H. Staelin & E.C. Reifenstein, Pulsating Radio Sources near the Crab Nebula, Science, 1968, Volume 162, Issue 3861, pp. 1481-1483

[6] I. Cognard et al., Giant Radio Pulses from a Millisecond Pulsar, 1996, ApJL 457, L81

[7] https://casper.berkeley.edu/wiki/ROACH.

[8] R.Weber et al. Data preprocessing for decametre wavelength exoplanet detection: an example of cyclostationary RFI detector, EUSIPCO'2007,Poznan, Poland, August 2007.

[9] G.M. Nita et al, Radio Frequency Interference Excision Using Spectral-Domain Statistics, Astronomical Society of the Pacific, Vol. 119, No. 857, pp. 805-827, July 2007.

[10] S. Deans, "The radon transform and some of its applications ", Krieger Pub. Co., 1983

[11] G. Desvignes, PhD thesis "L'observation des pulsars au Radiotélescope de Nançay. Applications à la recherche de nouveaux objets, à l'étude des systèmes binaires relativistes et à la détection d'un fond d'ondes gravitationnelles ", University of Orléans, 2009.